UAV-Mounted Multi-Functional RIS for Combating Eavesdropping in Wireless Networks

Wen Wang, Wanli Ni, *Graduate Student Member, IEEE*, Hui Tian, *Senior Member, IEEE*, Yonina C. Eldar, *Fellow, IEEE*, and Dusit Niyato, *Fellow, IEEE*

***Abstract*—In this letter, we propose an unmanned aerial vehicle (UAV)-mounted multi-functional reconfigurable intelligent surface (MF-RIS) to combat an eavesdropping attack. The proposed UAV-mounted MF-RIS is capable of reflecting and amplifying the desired signal, and emitting the friendly jamming (i.e., artificial noise) simultaneously. As such, the signal received at the legitimate user is significantly enhanced, while destructive interference is generated at the eavesdropper (Eve). In the presence of multiple Eves, we maximize the secrecy rate by jointly optimizing the transmit beamforming at the base station, the reflection matrix, and the deployment location of MF-RIS. Then, we propose an iterative algorithm to solve this non-convex problem efficiently. Simulation results show that, through the joint design of UAV and RIS architectures, the proposed MF-RIS can effectively combat eavesdropping and achieve more secure communications compared with existing passive or active RISs.**

***Index Terms*—Multi-functional RIS, unmanned aerial vehicle (UAV), friendly jamming, secure communications.**

I. Introduction

DUE TO the broadcast nature of radio channels, wireless communications face the problem of information leakage, especially in the presence of malicious eavesdroppers (Eves) [1]. Although some existing technologies, such as unmanned aerial vehicle (UAV) [2] and reconfigurable intelligent surface (RIS) [3], can enhance secure communication performance to a certain extent by adjusting signal propagation or adding artificial noise, the separate design of these techniques makes it challenging to unleash their full potential. To this end, it is desirable to develop a new UAV-mounted RIS architecture that judiciously combines the aforementioned techniques, so as to effectively combat eavesdropping over the air.

In the literature, some prior works have adopted UAV and/or RIS to safeguard wireless communications between the base station (BS) and users [3], [4], [5], [6], [7], [8]. As summarized in Table I, the authors of [3] deployed a UAV-mounted passive RIS to relay the signal from the BS to the legitimate user (Bob), in the presence of multiple Eves. Considering the severe path loss of legitimate cascaded links, active RISs were proposed in [4] to enhance the secure transmission by amplifying the reflective signal. However, numerical results in [5] revealed that relying on RISs alone is insufficient to deal with the increasing number of Eves due to the lack of spatial degrees of freedom (DoFs). To degrade the channel quality of potential Eves, the authors of [5], [6], [7], [8] exploited the benefits of ground and aerial jamming in safeguarding communications. Nevertheless, the ground-based designs in [5] and [6] were limited to terrestrial RIS scenarios where the RIS location is fixed. The UAV in [7] played the role of a BS or jammer, and only one Eve was considered in [6] and [7]. Although an aerial platform carrying an RIS and a friendly jammer was employed in [8], the jammer relies on another fixed RIS to manipulate the signal. From Table I, we observe that most existing works focus on the independent design and optimization of UAV and RIS. So far, how to integrate the hardware of UAV and RIS and efficiently optimize this new joint architecture is still an open problem.

TABLE I

Comparison of This Letter With Other Representative Works

Properties \ References	[3]	[4]	[5]	[6]	[7]	[8]	**This paper**
Joint UAV-RIS design							✓
Signal amplification		✓		✓			✓
Friendly jamming			✓	✓	✓	✓	✓
Multiple eavesdroppers	✓		✓			✓	✓

Here, we propose a UAV-mounted multi-functional RIS (MF-RIS) to safeguard wireless communications in the presence of multiple Eves. Specifically, the MF-RIS controller can control each element to switch between the amplification mode (A mode) and the jamming mode (J mode). These elements operating in A mode reflect and amplify the incident signal, while the elements in J mode emit the jamming signal generated by the UAV. In this way, the proposed MF-RIS is able to enhance desired reception and combat malicious eavesdropping simultaneously. Unlike amplify-and-forward relays which require power-consuming radio frequency chains, the MF-RIS realizes signal amplification by using low-power negative resistance components, such as tunnel diodes [4]. The main contributions of this letter are summarized as follows:

- To fully exploit the advantages of UAV and RIS, we design a new MF-RIS architecture that integrates signal reflection, amplification, and friendly jamming (i.e., artificial noise) into a UAV-mounted metasurface.
- By jointly optimizing the transmit beamforming and the MF-RIS deployment, we formulate a resource allocation problem to maximize the secrecy rate. Then, an iterative algorithm is proposed to solve the resulting mixed-integer non-linear programming (MINLP) problem efficiently.

Manuscript received 28 March 2023; revised 18 May 2023; accepted 5 June 2023. Date of publication 8 June 2023; date of current version 9 October 2023. The work of Hui Tian was supported by the National Key Research and Development Program of China under Grant 2020YFB1807801. The work of Wen Wang was supported in part by the Beijing University of Posts and Telecommunications (BUPT) Excellent Ph.D. Students Foundation under Grant CX2022103, and in part by the China Scholarship Council. The associate editor coordinating the review of this article and approving it for publication was H. Lee. *(Corresponding author: Hui Tian.)*

Wen Wang, Wanli Ni, and Hui Tian are with the State Key Laboratory of Networking and Switching Technology, Beijing University of Posts and Telecommunications, Beijing 100876, China (e-mail: wen.wang@bupt.edu.cn; charleswall@bupt.edu.cn; tianhui@bupt.edu.cn).

Yonina C. Eldar is with the Faculty of Mathematics and Computer Science, Weizmann Institute of Science, Rehovot 7610001, Israel (e-mail: yonina.eldar@weizmann.ac.il).

Dusit Niyato is with the School of Computer Science and Engineering, Nanyang Technological University, Singapore 117543 (e-mail: dniyato@ntu.edu.sg).

Digital Object Identifier 10.1109/LWC.2023.3283981

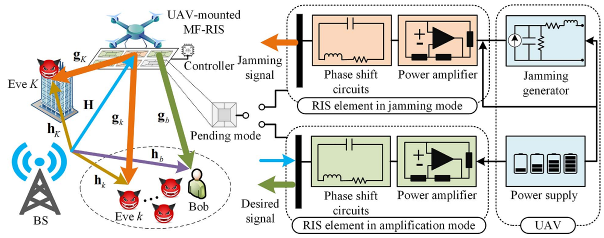

Fig. 1. Illustration of combating eavesdropping via UAV-mounted MF-RIS.

- Simulation results show that the MF-RIS prefers to be deployed in proximity to Eves and provides up to 300% higher secrecy rate than that of passive and active RISs.

II. System Model and Problem Formulation

A. System Model

As shown in Fig. 1, we consider a UAV-mounted MF-RIS assisted secure communication system, where an N-antenna BS transmits signals to a single-antenna Bob in the presence of K single-antenna independent Eves. The set of Eves is denoted by $\mathcal{K} = \{1, \ldots, K\}$. We assume that Eves are active users in the considered system but are not trusted by Bob [4]. The fixed three-dimensional (3D) locations of the BS, Bob, and Eves are denoted by $\mathbf{w}_0 = [x_0, y_0, z_0]^{\mathrm{T}}$ and $\mathbf{w}_i = [x_i, y_i, z_i]^{\mathrm{T}}, \forall i \in \{b\} \cup \mathcal{K}$, respectively. The height of the K-th Eve is h, while the BS, Bob, and other Eves are located on the ground, i.e., $z_0 = z_i = 0, \forall i \in \{b, 1, \ldots, K-1\}$, and $z_K = h$. Moreover, the location of the UAV-mounted MF-RIS is $\mathbf{w} = [x, y, z]^{\mathrm{T}}$, satisfying $\mathbf{w} \in \mathcal{W} = \{[x, y, z]^{\mathrm{T}} | x_{\min} \le x \le x_{\max}, y_{\min} \le y \le y_{\max}, z_{\min} \le z \le z_{\max}\}$, where $[x_{\min}, x_{\max}]$, $[y_{\min}, y_{\max}]$, and $[z_{\min}, z_{\max}]$ are the candidate ranges along 3D coordinates.

We assume that the MF-RIS is equipped with M elements, forming an $M = M_x \times M_y$ uniform rectangular array. The set of elements is denoted by $\mathcal{M} = \{1, \ldots, M\}$. The coefficients for the A and J modes are given by $\Theta_{\mathrm{A}} = \mathbf{A}\Theta$ and $\Theta_{\mathrm{J}} = (\mathbf{I}_M - \mathbf{A})\Theta$, respectively, with $\mathbf{A} = \mathrm{diag}(\alpha_1, \ldots, \alpha_M)$ and $\Theta = \mathrm{diag}(\sqrt{\beta_1} e^{j\theta_1}, \ldots, \sqrt{\beta_M} e^{j\theta_M})$. Here, $\alpha_m \in \{0, 1\}$, $\beta_m \in [0, \beta_{\max}]$, and $\theta_m \in [0, 2\pi)$ denote the mode indicator, the amplitude, and the phase shift of the m-th element, respectively. In particular, $\alpha_m = 1$ indicates that the m-th element is in A mode, while $\alpha_m = 0$ indicates that it is in J mode, and $\beta_{\max} \ge 1$ is the maximum amplification factor.

To characterize the performance limit of the considered system, we assume that the channel state information of all involved channel links is perfectly known at the BS by using existing channel estimation methods [9]. We adopt Rician fading for all communication links [3]. Then, the channel from the BS to the MF-RIS is given by

$$\mathbf{H} = \sqrt{\frac{h_0}{d_0^{\kappa_0}}} \left(\sqrt{\frac{\rho}{\rho+1}} \mathbf{H}^{\mathrm{L}} + \sqrt{\frac{1}{\rho+1}} \mathbf{H}^{\mathrm{NL}} \right), \tag{1}$$

where h_0 is the channel gain with a distance of 1 meter (m), $d_0 = \|\mathbf{w} - \mathbf{w}_0\|$ is the distance between the BS and the MF-RIS, κ_0 is the corresponding path loss exponent, ρ is the Rician factor, and $\mathbf{H}^{\mathrm{NL}}$ is the non-LoS component modeled as Rayleigh fading. Here, $\mathbf{H}^{\mathrm{L}}$ is the deterministic LoS component related to the angle of departures (AoDs) and angle of arrivals (AoAs) of this link [3]. The channels from the MF-RIS to Bob/Eves and from the BS to Bob/Eves, denoted by $\mathbf{g}_i$ and $\mathbf{h}_i$, are modeled similarly. In particular, $\mathbf{g}_i$ is given by $\mathbf{g}_i = \sqrt{\frac{h_0}{d_i^{\kappa_i}}} (\sqrt{\frac{\rho}{\rho+1}} \mathbf{g}_i^{\mathrm{L}} + \sqrt{\frac{1}{\rho+1}} \mathbf{g}_i^{\mathrm{NL}})$, with $d_i = \|\mathbf{w}_i - \mathbf{w}\|$. Here, we define $\bar{\mathbf{h}}_i = \mathbf{h}_i^{\mathrm{H}} + \mathbf{g}_i^{\mathrm{H}} \Theta_{\mathrm{A}} \mathbf{H}$ as the combined channel.

Denoting $\mathbf{f}$ as the confidential beamforming vector and $s \sim \mathcal{CN}(0, 1)$ as the modulated symbol, the signal received at Bob and Eves is given by

$$y_i = \bar{\mathbf{h}}_i \mathbf{f} s + \mathbf{g}_i^{\mathrm{H}} \Theta_{\mathrm{J}} \mathbf{z} + \mathbf{g}_i^{\mathrm{H}} \Theta \mathbf{n}_{\mathrm{s}} + n_0, \ \forall i \in \{b\} \cup \mathcal{K}, \tag{2}$$

where $\mathbf{z} \sim \mathcal{CN}(\mathbf{0}, P_{\mathrm{J}} \mathbf{I}_M)$ is the jamming vector with power P_{J}, $\mathbf{n}_s \sim \mathcal{CN}(\mathbf{0}, \sigma_1^2 \mathbf{I}_M)$ denotes the amplification noise introduced at the MF-RIS with per-element noise power σ_1^2, and $n_0 \sim \mathcal{CN}(0, \sigma_0^2)$ is the additive white Gaussian noise (AWGN) with mean zero and variance σ_0^2 received at users. The achievable data rate of Bob and Eves is then given by

$$R_i = \log_2 \left(1 + \frac{|\bar{\mathbf{h}}_i \mathbf{f}|^2}{P_{\mathrm{J}} \|\mathbf{g}_i^{\mathrm{H}} \Theta_{\mathrm{J}}\|^2 + \sigma_1^2 \|\mathbf{g}_i^{\mathrm{H}} \Theta\|^2 + \sigma_0^2} \right), \ \forall i. \tag{3}$$

B. Problem Formulation

Our goal is to maximize the secrecy rate by jointly optimizing the transmit beamforming at the BS, the coefficient matrix and 3D location of the UAV-mounted MF-RIS. Mathematically, the optimization problem is formulated as

$$\max_{\mathbf{f}, \mathbf{A}, \Theta, \mathbf{w}} \ \left[R_b - \max_{k \in \mathcal{K}} R_k \right]^+ \tag{4a}$$

$$\text{s.t.} \quad \|\Theta_{\mathrm{A}} \mathbf{H} \mathbf{f}\|^2 + P_{\mathrm{J}} \|\Theta_{\mathrm{J}}\|_F^2 + \sigma_1^2 \|\Theta\|_F^2 \le P_{\mathrm{out}}, \tag{4b}$$

$$\alpha_m \in \{0, 1\}, \beta_m \in [0, \beta_{\max}], \theta_m \in [0, 2\pi), \ \forall m, \tag{4c}$$

$$\|\mathbf{f}\|^2 \le P_{\max}, \ \mathbf{w} \in \mathcal{W}, \tag{4d}$$

where $[\cdot]^+ \triangleq \max\{x, 0\}$ and we omit $[\,\cdot\,]^+$ in the following, due to the non-negative nature of the optimal secrecy rate. Here, P_{out} and $P_{\max}$ denote the power budget at the UAV and the BS, respectively. Due to the fact that α_m is binary and other variables are continuous, problem (4) is an MINLP problem, which is difficult to solve optimally. In the following, we propose an iterative algorithm to solve it efficiently.

III. Proposed Solutions

A. Transmit Beamforming Optimization

Given $\mathbf{A}$, Θ, and $\mathbf{w}$, we first handle the highly coupled objective function (4a). We introduce slack variables E_i and F_i, satisfying $E_i^{-1} = |\bar{\mathbf{h}}_i \mathbf{f}|^2$ and $F_i = P_{\mathrm{J}} \|\mathbf{g}_i^{\mathrm{H}} \Theta_{\mathrm{J}}\|^2 + \sigma_1^2 \|\mathbf{g}_i^{\mathrm{H}} \Theta\|^2 + \sigma_0^2$. Then, (4a) is rewritten as

$$\log_2(1 + E_b^{-1} F_b^{-1}) - \max\nolimits_{k \in \mathcal{K}} \log_2(1 + E_k^{-1} F_k^{-1}). \tag{5}$$

Since (5) is still non-concave, we resort to the successive convex approximation (SCA) method to tackle it. Specifically, we use the first-order Taylor expansion (FTS) as a lower-bound to approximate R_b, i.e., $R_b^{\mathrm{lb}} = \log_2 (\frac{E_b^{(\ell)} F_b^{(\ell)} + 1}{E_b^{(\ell)} F_b^{(\ell)}}) - \frac{(\log_2 e)(E_b - E_b^{(\ell)})}{E_b^{(\ell)} + (E_b^{(\ell)})^2 F_b^{(\ell)}} - \frac{(\log_2 e)(F_b - F_b^{(\ell)})}{F_b^{(\ell)} + (F_b^{(\ell)})^2 E_b^{(\ell)}}$, where $\{E_b^{(\ell)}, F_b^{(\ell)}\}$ is the feasible point in the ℓ-th iteration.

We further define $\bar{\mathbf{H}}_i = \bar{\mathbf{h}}_i^{\mathrm{H}} \bar{\mathbf{h}}_i$, $\bar{\mathbf{H}} = \mathbf{H}^{\mathrm{H}} \Theta_{\mathrm{A}}^{\mathrm{H}} \Theta_{\mathrm{A}} \mathbf{H}$, and $\mathbf{F} = \mathbf{f}\mathbf{f}^{\mathrm{H}}$, satisfying $\mathbf{F} \succeq \mathbf{0}$ and $\mathrm{rank}(\mathbf{F}) = 1$. Then, the transmit beamforming subproblem is formulated as

$$\max_{\mathbf{F}, E_i, F_i} \quad R_b^{\mathrm{lb}} - \max_{k \in \mathcal{K}} R_k \tag{6a}$$

$$\text{s.t.} \quad \mathrm{Tr}(\mathbf{F}) \le P_{\max}, \ \mathbf{F} \succeq \mathbf{0}, \ \mathrm{rank}(\mathbf{F}) = 1, \tag{6b}$$

$$\mathrm{Tr}(\bar{\mathbf{H}} \mathbf{F}) + P_{\mathrm{J}} \|\Theta_{\mathrm{J}}\|_F^2 + \sigma_1^2 \|\Theta\|_F^2 \le P_{\mathrm{out}}, \tag{6c}$$

$$E_b^{-1} \le \mathrm{Tr}(\bar{\mathbf{H}}_b \mathbf{F}), E_k^{-1} \ge \mathrm{Tr}(\bar{\mathbf{H}}_k \mathbf{F}), \ \forall k, \tag{6d}$$

$$F_b \ge P_{\mathrm{J}} \|\mathbf{g}_b^{\mathrm{H}} \Theta_{\mathrm{J}}\|^2 + \sigma_1^2 \|\mathbf{g}_b^{\mathrm{H}} \Theta\|^2 + \sigma_0^2, \tag{6e}$$

$$F_k \le P_{\mathrm{J}} \|\mathbf{g}_k^{\mathrm{H}} \Theta_{\mathrm{J}}\|^2 + \sigma_1^2 \|\mathbf{g}_k^{\mathrm{H}} \Theta\|^2 + \sigma_0^2, \ \forall k. \tag{6f}$$

Algorithm 1 The SROCR-Based Algorithm for Solving (6)

1: **Initialization:** set initial iteration index $\ell = 0$, initialize $\{\mathbf{F}^{(0)}, \upsilon^{(0)}\}$ and step size $\delta^{(0)}$.
2: **repeat**
3: **If** (9) is feasible, update $\mathbf{F}^{(\ell+1)}$ by solving (9) and update $\delta^{(\ell+1)} = \delta^{(\ell)}$;
4: **Else** update $\delta^{(\ell+1)} = \frac{\delta^{(\ell)}}{2}$;
5: Update $\upsilon^{(\ell+1)} = \min\left(1, \frac{\lambda_{\max}(\mathbf{F}^{(\ell+1)})}{\mathrm{Tr}(\mathbf{F}^{(\ell+1)})} + \delta^{(\ell+1)}\right)$;
6: Update $\ell = \ell + 1$;
7: **until** the stopping criterion is met.

The difficulty of solving (6) lies in the rank-one constraint in (6b) and the non-convex constraint $E_k^{-1} \geq \mathrm{Tr}(\bar{\mathbf{H}}_k \mathbf{F})$ in (6d). To deal with the rank-one constraint, we adopt the sequential rank-one constraint relaxation (SROCR) method. Unlike the semidefinite relaxation (SDR) method that drops the constraint directly, SROCR gradually relaxes the constraint to obtain a feasible rank-one solution [10]. Simulation results in [11] have shown the performance gains of SROCR over SDR. Defining $\upsilon^{(\ell-1)} \in [0, 1]$ as the relaxation parameter in the ℓ-th iteration, this constraint in the ℓ-th iteration is relaxed as

$$\left(\mathbf{f}^{\mathrm{eig},(\ell-1)}\right)^{\mathrm{H}} \mathbf{F}^{(\ell)} \mathbf{f}^{\mathrm{eig},(\ell-1)} \geq \upsilon^{(\ell-1)} \mathrm{Tr}(\mathbf{F}^{(\ell)}), \tag{7}$$

where $\mathbf{f}^{\mathrm{eig},(\ell-1)}$ denotes the eigenvector corresponding to the largest eigenvalue of $\mathbf{F}^{(\ell-1)}$, and $\mathbf{F}^{(\ell-1)}$ is the obtained solution in the $(\ell-1)$-th iteration.

Replacing the non-convex part E_k^{-1} with its FTS, $(E_k^{-1})^{\mathrm{lb}} = (2E_k^{(\ell)} - E_k)(E_k^{(\ell)})^{-2}$, constraint $E_k^{-1} \geq \mathrm{Tr}(\bar{\mathbf{H}}_k \mathbf{F})$ is recast as

$$(E_k^{-1})^{\mathrm{lb}} \geq \mathrm{Tr}(\bar{\mathbf{H}}_k \mathbf{F}). \tag{8}$$

Thus, problem (6) is transformed into

$$\max_{\mathbf{F}, E_i, F_i} \quad R_b^{\mathrm{lb}} - \max_{k \in \mathcal{K}} R_k \tag{9a}$$

$$\text{s.t.} \quad \mathrm{Tr}(\mathbf{F}) \leq P_{\max}, \ \mathbf{F} \succeq \mathbf{0}, \ E_b^{-1} \leq \mathrm{Tr}(\bar{\mathbf{H}}_b \mathbf{F}), \tag{9b}$$

$$\text{(6c), (6e), (6f), (7), (8).} \tag{9c}$$

Since problem (9) is a semidefinite program (SDP), it can be solved efficiently via CVX toolbox. Accordingly, the details of solving problem (6) are given in Algorithm 1.

B. MF-RIS Coefficient Design

Given $\mathbf{f}$ and $\mathbf{w}$, we denote $\mathbf{X} = \mathbf{x}\mathbf{x}^{\mathrm{H}}$, $\mathbf{X} \in \{\mathbf{U}_{\mathrm{A}}, \mathbf{U}_{\mathrm{J}}, \mathbf{U}\}$, $\mathbf{x} \in \{\mathbf{u}_{\mathrm{A}}, \mathbf{u}_{\mathrm{J}}, \mathbf{u}\}$, where $\mathbf{u}_{\mathrm{A}} \in \mathbb{C}^{(M+1)\times 1}$, $\mathbf{u}_{\mathrm{J}} \in \mathbb{C}^{M\times 1}$, and $\mathbf{u} \in \mathbb{C}^{M\times 1}$. The expressions of $\mathbf{X}$ and $\mathbf{x}$ are given in (10) at the bottom of this page. Here, $\mathbf{X}$ should satisfy the following constraints:

$$\mathbf{X} \succeq \mathbf{0}, \ \mathrm{rank}(\mathbf{X}) = 1, \ [\mathbf{U}_{\mathrm{A}}]_{M+1,M+1} = 1, \tag{11a}$$

$$[\mathbf{X}]_{m,m} = \begin{cases} \alpha_m^2 \beta_m, & \text{if } \mathbf{X} = \mathbf{U}_{\mathrm{A}}, \\ (1-\alpha_m)^2 \beta_m, & \text{if } \mathbf{X} = \mathbf{U}_{\mathrm{J}}, \\ \beta_m, & \text{if } \mathbf{X} = \mathbf{U}. \end{cases} \tag{11b}$$

We further define $\widetilde{\mathbf{h}}_i = [\mathrm{diag}(\mathbf{g}_i^{\mathrm{H}})\mathbf{H}; \mathbf{h}_i^{\mathrm{H}}]\mathbf{f}$ and $\widetilde{\mathbf{h}} = [\mathbf{H}; \mathbf{0}_{1\times N}]\mathbf{f}$. Then, (4) is reduced to

$$\max_{\mathbf{X}, E_i, F_i} \quad R_b^{\mathrm{lb}} - \max_{k \in \mathcal{K}} R_k \tag{12a}$$

$$\text{s.t.} \quad E_b^{-1} \leq \mathrm{Tr}(\widetilde{\mathbf{H}}_b \mathbf{U}_{\mathrm{A}}), (E_k^{-1})^{\mathrm{lb}} \geq \mathrm{Tr}(\widetilde{\mathbf{H}}_k \mathbf{U}_{\mathrm{A}}), \forall k, \tag{12b}$$

$$F_b \geq \mathrm{Tr}((P_{\mathrm{J}} \mathbf{U}_{\mathrm{J}} + \sigma_1^2 \mathbf{U})\mathbf{G}_b) + \sigma_0^2, \tag{12c}$$

$$F_k \leq \mathrm{Tr}((P_{\mathrm{J}} \mathbf{U}_{\mathrm{J}} + \sigma_1^2 \mathbf{U})\mathbf{G}_k) + \sigma_0^2, \ \forall k, \tag{12d}$$

$$\mathrm{Tr}(\widetilde{\mathbf{H}} \mathbf{U}_{\mathrm{A}}) + P_{\mathrm{J}} \mathrm{Tr}(\mathbf{U}_{\mathrm{J}}) + \sigma_1^2 \mathrm{Tr}(\mathbf{U}) \leq P_{\mathrm{out}}, \tag{12e}$$

$$\alpha_m \in \{0, 1\}, \beta_m \in [0, \beta_{\max}], \forall m, \text{(11a), (11b)}, \tag{12f}$$

where $\widetilde{\mathbf{H}}_i = \widetilde{\mathbf{h}}_i \widetilde{\mathbf{h}}_i^{\mathrm{H}}$, $\widetilde{\mathbf{H}} = \widetilde{\mathbf{h}} \widetilde{\mathbf{h}}^{\mathrm{H}}$, and $\mathbf{G}_i = \mathbf{g}_i \mathbf{g}_i^{\mathrm{H}}$. Problem (12) is non-convex due to the binary constraint in (12f), the rank-one constraint in (11a), and the highly coupled constraint (11b). The binary constraint is equivalently transformed into the following continuous ones:

$$\alpha_m - \alpha_m^2 \leq 0, \ 0 \leq \alpha_m \leq 1, \ \forall m. \tag{13}$$

For the non-convex part $-\alpha_m^2$, the FTS is again performed to obtain a linear upper-bound at the feasible point $\{\alpha_m^{(\ell)}\}$, which is given by $(-\alpha_m^{(\ell)})^{\mathrm{ub}} = -2\alpha_m^{(\ell)} \alpha_m + (\alpha_m^{(\ell)})^2$.

Similar to the transformation for constraint $\mathrm{rank}(\mathbf{F}) = 1$ in Section III-A, we handle the rank-one constraint $\mathrm{rank}(\mathbf{X}) = 1$ using SROCR. By defining $w^{(\ell-1)} \in [0, 1]$, $\mathbf{x}^{\mathrm{eig},(\ell-1)}$, and $\mathbf{X}^{(\ell-1)}$ to correspond to $\upsilon^{(\ell-1)} \in [0, 1]$, $\mathbf{f}^{\mathrm{eig},(\ell-1)}$, and $\mathbf{F}^{(\ell-1)}$ in (7), this constraint in the ℓ-th iteration is relaxed as

$$\left(\mathbf{x}^{\mathrm{eig},(\ell-1)}\right)^{\mathrm{H}} \mathbf{X}^{(\ell)} \mathbf{x}^{\mathrm{eig},(\ell-1)} \geq w^{(\ell-1)} \mathrm{Tr}(\mathbf{X}^{(\ell)}). \tag{14}$$

The non-convexity of constraint (11b) arises from the highly coupled terms $\alpha_m^2 \beta_m$ and $(1-\alpha_m)^2 \beta_m$. Using the penalty function method, with the introduced slack variables $\xi_{m,\mathrm{A}}$ and $\xi_{m,\mathrm{J}}$, (11b) is equivalently recast as

$$[\mathbf{X}]_{m,m} = \begin{cases} \xi_{m,\mathrm{A}}, & \text{if } \mathbf{X} = \mathbf{U}_{\mathrm{A}}, \\ \xi_{m,\mathrm{J}}, & \text{if } \mathbf{X} = \mathbf{U}_{\mathrm{J}}, \\ \beta_m, & \text{if } \mathbf{X} = \mathbf{U}, \end{cases} \tag{15a}$$

$$\xi_{m,\mathrm{A}} \leq \alpha_m^2 \beta_m, \ \xi_{m,\mathrm{J}} \leq (1-\alpha_m)^2 \beta_m, \tag{15b}$$

$$\xi_{m,\mathrm{A}} \geq \alpha_m^2 \beta_m, \ \xi_{m,\mathrm{J}} \geq (1-\alpha_m)^2 \beta_m. \tag{15c}$$

For the non-convex constraints in (15b), we apply the FTS at the feasible point $\{\alpha_m^{(\ell)}, \beta_m^{(\ell)}\}$ obtained in the ℓ-th iteration. These constraints are then approximated by

$$\xi_{m,\mathrm{A}} \leq \xi_{m,\mathrm{A}}^{\mathrm{ub}}, \ \xi_{m,\mathrm{J}} \leq \xi_{m,\mathrm{J}}^{\mathrm{ub}}, \tag{16}$$

where $\xi_{m,\mathrm{A}}^{\mathrm{ub}} = 2(\alpha_m - \alpha_m^{(\ell)})\alpha_m^{(\ell)} \beta_m^{(\ell)} + (\alpha_m^{(\ell)})^2 \beta_m$ and $\xi_{m,\mathrm{J}}^{\mathrm{ub}} = (\beta_m - \beta_m \alpha_m^{(\ell)} - 2\beta_m^{(\ell)}(\alpha_m - \alpha_m^{(\ell)}))(1 - \alpha_m^{(\ell)})$. We next adopt the convex upper bound (CUB) substitution to deal with (15c). Define functions $f(\alpha, \beta) = \alpha^2 \beta$ and $g(\alpha, \beta) = \frac{C}{2}\alpha^4 + \frac{\beta^2}{2C}$. Then, it is proved that $g(\alpha, \beta)$ is a convex overestimate of $f(\alpha, \beta)$ for $\alpha, \beta, C > 0$. The equations $f(\alpha, \beta) = g(\alpha, \beta)$ and $\nabla f(\alpha, \beta) = \nabla g(\alpha, \beta)$ hold when $C = \frac{\beta}{\alpha^2}$, where ∇f is the gradient of f. Thus, by replacing the non-convex terms with their CUBs, constraints in (15c) are transformed into

$$\xi_{m,\mathrm{A}} \geq \xi_{m,\mathrm{A}}^{\mathrm{lb}}, \ \xi_{m,\mathrm{J}} \geq \xi_{m,\mathrm{J}}^{\mathrm{lb}}, \tag{17}$$

where $\xi_{m,\mathrm{A}}^{\mathrm{lb}} = \frac{C_{m,\mathrm{A}} \alpha_m^4}{2} + \frac{\beta_m^2}{2C_{m,\mathrm{A}}}$ and $\xi_{m,\mathrm{J}}^{\mathrm{lb}} = \frac{C_{m,\mathrm{J}}(1-\alpha_m)^4}{2} + \frac{\beta_m^2}{2C_{m,\mathrm{J}}}$. The fixed points $C_{m,\mathrm{A}}$ and $C_{m,\mathrm{J}}$ in the ℓ-th iteration

$$\mathbf{X} = \begin{cases} \mathbf{u}_{\mathrm{A}} \mathbf{u}_{\mathrm{A}}^{\mathrm{H}}, & \text{if } \mathbf{X} = \mathbf{U}_{\mathrm{A}}, \\ \mathbf{u}_{\mathrm{J}} \mathbf{u}_{\mathrm{J}}^{\mathrm{H}}, & \text{if } \mathbf{X} = \mathbf{U}_{\mathrm{J}}, \\ \mathbf{u}\mathbf{u}^{\mathrm{H}}, & \text{if } \mathbf{X} = \mathbf{U}, \end{cases} \quad \mathbf{x} = \begin{cases} \left[\alpha_1 \sqrt{\beta_1} e^{-j\theta_1}; \ldots; \alpha_M \sqrt{\beta_M} e^{-j\theta_M}; 1\right], & \text{if } \mathbf{x} = \mathbf{u}_{\mathrm{A}}, \\ \left[(1-\alpha_1)\sqrt{\beta_1} e^{-j\theta_1}; \ldots; (1-\alpha_M)\sqrt{\beta_M} e^{-j\theta_M}\right], & \text{if } \mathbf{x} = \mathbf{u}_{\mathrm{J}}, \\ \left[\sqrt{\beta_1} e^{-j\theta_1}; \ldots; \sqrt{\beta_M} e^{-j\theta_M}\right], & \text{if } \mathbf{x} = \mathbf{u}. \end{cases} \tag{10}$$

are updated by $C_{m,\mathrm{A}}^{(\ell)} = \frac{\beta_m^{(\ell-1)}}{(\alpha_m^{(\ell-1)})^2}$ and $C_{m,\mathrm{J}}^{(\ell)} = \frac{\beta_m^{(\ell-1)}}{(1-\alpha_m^{(\ell-1)})^2}$, respectively.

As a result, problem (12) is reformulated as

$$\max_{\Delta_1} R_b^{\mathrm{lb}} - \max_{k\in\mathcal{K}} R_k - \mu^{(\ell)} G(b_m, \bar{b}_m, c_m, \bar{c}_m) \tag{18a}$$

$$\text{s.t.}\ \xi_{m,\mathrm{A}} \le \xi_{m,\mathrm{A}}^{\mathrm{ub}} + b_m,\ \xi_{m,\mathrm{J}} \le \xi_{m,\mathrm{J}}^{\mathrm{ub}} + \bar{b}_m,\ \forall m, \tag{18b}$$

$$\xi_{m,\mathrm{A}} + c_m \ge \xi_{m,\mathrm{A}}^{\mathrm{lb}},\ \xi_{m,\mathrm{J}} + \bar{c}_m \ge \xi_{m,\mathrm{J}}^{\mathrm{lb}},\ \forall m, \tag{18c}$$

$$\beta_m \in [0, \beta_{\max}],\ 0 \le \alpha_m \le 1,\ \forall m, \tag{18d}$$

$$\mathbf{X} \succeq \mathbf{0},\ [\mathbf{U}_\mathrm{A}]_{M+1,M+1} = 1, \tag{18e}$$

$$\alpha_m + (-\alpha_m^{(\ell)})^{\mathrm{ub}} \le 0, \forall m, \text{(12b)-(12e), (14), (15a)}, \tag{18f}$$

where $\Delta_1 = \{\mathbf{X}, E_i, F_i, b_m, \bar{b}_m, c_m, \bar{c}_m, \xi_{m,\mathrm{A}}, \xi_{m,\mathrm{J}}, \forall i, m\}$. Here, $G(b_m, \bar{b}_m, c_m, \bar{c}_m) = \sum_{m=1}^{M}(b_m + \bar{b}_m + c_m + \bar{c}_m)$ is the penalty term added into the objective function, which is scaled by the multiplier $\mu^{(\ell)}$ in ℓ-th iteration. Considering that problem (18) is an SDP, we can adopt the CVX toolbox to solve it efficiently. The algorithm for solving (12) can be extended from Algorithm 1 and is omitted here for brevity.

C. MF-RIS Location Optimization

Given $\mathbf{f}$, $\mathbf{A}$, and Θ, the MF-RIS location optimization subproblem is formulated as

$$\max_{\mathbf{w}, E_i, F_i} R_b^{\mathrm{lb}} - \max_{k\in\mathcal{K}} R_k \tag{19a}$$

$$\text{s.t.}\ E_b^{-1} \le |\bar{\mathbf{h}}_b \mathbf{f}|^2,\ (E_k^{-1})^{\mathrm{lb}} \ge |\bar{\mathbf{h}}_k \mathbf{f}|^2,\ \forall k, \tag{19b}$$

$$F_b \ge P_\mathrm{J}\|\mathbf{g}_b^\mathrm{H}\Theta_\mathrm{J}\|^2 + \sigma_1^2\|\mathbf{g}_b^\mathrm{H}\Theta\|^2 + \sigma_0^2, \tag{19c}$$

$$F_k \le P_\mathrm{J}\|\mathbf{g}_k^\mathrm{H}\Theta_\mathrm{J}\|^2 + \sigma_1^2\|\mathbf{g}_k^\mathrm{H}\Theta\|^2 + \sigma_0^2, \forall k, \tag{19d}$$

$$\mathbf{w} \in \mathcal{W},\ \text{(4b)}. \tag{19e}$$

Following [3], $\mathbf{H}^\mathrm{L}$ and $\mathbf{g}_i^\mathrm{L}$ are related to the AoDs and AoAs of the BS-RIS and RIS-user links, respectively, which are non-linear and complex w.r.t. $\mathbf{w}$ and thus make (19) intractable. To tackle it, the $\mathbf{w}$ obtained in the $(\ell-1)$-iteration is used to approximate $\mathbf{H}^\mathrm{L}$ and $\mathbf{g}_i^\mathrm{L}$ in the ℓ-th iteration. Defining $\grave{\mathbf{H}} = \sqrt{\frac{\rho h_0}{\rho+1}}\mathbf{H}^\mathrm{L} + \sqrt{\frac{h_0}{\rho+1}}\mathbf{H}^\mathrm{NL}$ and $\grave{\mathbf{g}}_i = \sqrt{\frac{\rho h_0}{\rho+1}}\mathbf{g}_i^\mathrm{L} + \sqrt{\frac{h_0}{\rho+1}}\mathbf{g}_i^\mathrm{NL}$, constraints (19b)-(19d) and (4b) are rewritten as

$$\bar{P}_{\mathrm{out}} \ge d_0^{-\kappa_0} g_0, E_b^{-1} \le \mathbf{d}_b\mathbf{D}_b\mathbf{d}_b^\mathrm{T}, (E_k^{-1})^{\mathrm{lb}} \ge \mathbf{d}_k\mathbf{D}_k\mathbf{d}_k^\mathrm{T}, \tag{20a}$$

$$F_b \ge d_b^{-\kappa_b} g_b + \sigma_0^2,\ F_k \le d_k^{-\kappa_k} g_k + \sigma_0^2, \tag{20b}$$

where

$$g_0 = \|\Theta_\mathrm{A}\grave{\mathbf{H}}^{(\ell-1)}\mathbf{f}\|^2, \bar{P}_{\mathrm{out}} = P_{\mathrm{out}} - P_\mathrm{J}\|\Theta_\mathrm{J}\|_F^2 - \sigma_1^2\|\Theta\|_F^2,$$

$$\mathbf{d}_i = [1, d_0^{\frac{-\kappa_0}{2}} d_i^{\frac{-\kappa_i}{2}}], g_i = P_\mathrm{J}\|(\grave{\mathbf{g}}_i^{(\ell-1)})^\mathrm{H}\Theta_\mathrm{J}\|^2 + \sigma_1^2\|(\grave{\mathbf{g}}_i^{(\ell-1)})^\mathrm{H}\Theta\|^2,$$

$$\mathbf{D}_i = [\mathbf{h}_i, (\grave{\mathbf{H}}^{(\ell-1)})^\mathrm{H}\Theta_\mathrm{A}\grave{\mathbf{g}}_i^{(\ell-1)}]^\mathrm{H}\mathbf{f}\mathbf{f}^\mathrm{H}[\mathbf{h}_i, (\grave{\mathbf{H}}^{(\ell-1)})^\mathrm{H}\Theta_\mathrm{A}\grave{\mathbf{g}}_i^{(\ell-1)}].$$

Constraints (20a) and (20b) are still non-convex w.r.t. $\mathbf{w}$. Thus, we introduce a slack variable set $\Delta_2 = \{u, \bar{u}, t_i, s_i, e_i, r_i\}$, and define $\bar{\mathbf{d}}_i = [1, s_i]$, satisfying $u = \bar{u} = d_0^{-\frac{\kappa_0}{2}}$, $t_i = d_i^{-\frac{\kappa_i}{2}}$, $s_b = ut_b$, $s_k = \bar{u}t_k$, $e_i = d_i^{-\kappa_i}$, and $r_i = \bar{\mathbf{d}}_i\mathbf{D}_i\bar{\mathbf{d}}_i^\mathrm{T}$. And then, constraints (20a) and (20b) are transformed into

$$u \le d_0^{-\frac{\kappa_0}{2}}, t_b \le d_b^{-\frac{\kappa_b}{2}}, e_b \ge d_b^{-\kappa_b}, \bar{u} \ge d_0^{-\frac{\kappa_0}{2}},$$

$$t_k \ge d_k^{-\frac{\kappa_k}{2}}, e_k \le d_k^{-\kappa_k}, \tag{21a}$$

$$s_b \le ut_b,\ r_b \le \bar{\mathbf{d}}_b\mathbf{D}_b\bar{\mathbf{d}}_b^\mathrm{T},\ s_k \ge \bar{u}t_k,\ r_k \ge \bar{\mathbf{d}}_k\mathbf{D}_k\bar{\mathbf{d}}_k^\mathrm{T}, \tag{21b}$$

$$\bar{P}_{\mathrm{out}} \ge \bar{u}^2 g_0,\ E_b^{-1} \le r_b,\ F_b \ge e_b g_b + \sigma_0^2, \tag{21c}$$

$$(E_k^{-1})^{\mathrm{lb}} \ge r_k,\ F_k \le e_k g_k + \sigma_0^2. \tag{21d}$$

Constraints in (21a), constraints $r_b \le \bar{\mathbf{d}}_b\mathbf{D}_b\bar{\mathbf{d}}_b^\mathrm{T}$ and $s_k \ge \bar{u}t_k$ in (21b) are non-convex. The non-convexity of $s_k \ge \bar{u}t_k$ arises from its quasi-concave term $\bar{u}t_k$. Similar to the transformation for (15c) in Section III-B, we replace this term with its CUB $(\bar{u}t_k)^{\mathrm{ub}} = \frac{C_k\bar{u}^2}{2} + \frac{t_k^2}{2C_k}$, where C_k is updated by $C_k^{(\ell)} = \frac{t_k^{(\ell)}}{\bar{u}^{(\ell)}}$.

To facilitate the derivation of constraints in (21a), we unfold them as (22) as shown at the bottom of this page. The SCA method is adopted to handle $r_b \le \bar{\mathbf{d}}_b\mathbf{D}_b\bar{\mathbf{d}}_b^\mathrm{T}$ and (22). For the given point $\{\bar{\mathbf{d}}_b^{(\ell)}, u^{(\ell)}, t_b^{(\ell)}, e_b^{(\ell)}, \mathbf{w}^{(\ell)}\}$, the FTSs of $\bar{\mathbf{d}}_b\mathbf{D}_b\bar{\mathbf{d}}_b^\mathrm{T}$, $u^{-\frac{4}{\kappa_0}}$, $t_b^{-\frac{4}{\kappa_b}}$, $e_k^{-\frac{2}{\kappa_k}}$, x^2, y^2, and z^2 are given in (23) at the bottom of this page. Then, by replacing these terms with their FTSs given in (23), constraints $r_b \le \bar{\mathbf{d}}_b\mathbf{D}_b\bar{\mathbf{d}}_b^\mathrm{T}$ and (22) are rewritten as their convex approximations $r_b \le (\bar{\mathbf{d}}_b\mathbf{D}_b\bar{\mathbf{d}}_b^\mathrm{T})^{\mathrm{lb}}$ and $(23)'$. The expression of $(23)'$ is omitted here for brevity. Finally, problem (19) is recast as the following convex one:

$$\max_{\Delta_2, \mathbf{w}, E_i, F_i} R_b^{\mathrm{lb}} - \max_{k\in\mathcal{K}} R_k \tag{24a}$$

$$\text{s.t.}\ s_b \le ut_b,\ r_b \le (\bar{\mathbf{d}}_b\mathbf{D}_b\bar{\mathbf{d}}_b^\mathrm{T})^{\mathrm{lb}}, \tag{24b}$$

$$s_k \ge (\bar{u}t_k)^{\mathrm{ub}},\ r_k \ge \bar{\mathbf{d}}_k\mathbf{D}_k\bar{\mathbf{d}}_k^\mathrm{T},\ \forall k, \tag{24c}$$

$$\mathbf{w} \in \mathcal{W},\ \text{(21c)},\ \text{(21d)}, (23)'. \tag{24d}$$

The solution of problem (4) can be obtained by solving problems (6), (12), and (19) alternatively. Since the maximum transmit power is limited, the proposed algorithm is upper bounded and guaranteed to converge. The overall complexity is $\mathcal{O}(I_0(I_1(N^2+2K+2)^{3.5} + I_2(3M^2+8M+2K+3)^{3.5} + I_3(6K+11)^{3.5}))$, where I_0, I_1, I_2, and I_3 denote the number of outer iterations required for convergence, and the numbers of inner iterations required for solving (6), (12), and (19), respectively.

$$u^{-\frac{4}{\kappa_0}} - x^2 - x_0^2 - y^2 - y_0^2 - z^2 + 2(x_0 x + y_0 y) \ge 0,\quad t_b^{-\frac{4}{\kappa_b}} - x^2 - x_b^2 - y^2 - y_b^2 - z^2 + 2(x_b x + y_b y) \ge 0, \tag{22a}$$

$$x^2 + x_b^2 + y^2 + y_b^2 + z^2 - 2(x_b x + y_b y) - e_b^{-\frac{2}{\kappa_b}} \ge 0,\quad x^2 + x_0^2 + y^2 + y_0^2 + z^2 - 2(x_0 x + y_0 y) - \bar{u}^{-\frac{4}{\kappa_0}} \ge 0, \tag{22b}$$

$$x^2 + x_k^2 + y^2 + y_k^2 + z^2 + z_k^2 - 2(x_k x + y_k y + z_k z) - t_k^{-\frac{4}{\kappa_k}} \ge 0, \tag{22c}$$

$$e_k^{-\frac{2}{\kappa_k}} - x^2 - x_k^2 - y^2 - y_k^2 - z^2 - z_k^2 + 2(x_k x + y_k y + z_k z) \ge 0. \tag{22d}$$

$$(\bar{\mathbf{d}}_b\mathbf{D}_b\bar{\mathbf{d}}_b^\mathrm{T})^{\mathrm{lb}} = -\bar{\mathbf{d}}_b^{(\ell)}\mathbf{D}_b(\bar{\mathbf{d}}_b^{(\ell)})^\mathrm{T} + 2\Re\{\bar{\mathbf{d}}_b^{(\ell)}\mathbf{D}_b\bar{\mathbf{d}}_b^\mathrm{T}\},\quad (u^{-\frac{4}{\kappa_0}})^{\mathrm{lb}} = (u^{(\ell)})^{-\frac{4}{\kappa_0}} - \frac{4}{\kappa_0}(u - u^{(\ell)})(u^{(\ell)})^{-\frac{4}{\kappa_0}-1}, \tag{23a}$$

$$(t_b^{-\frac{4}{\kappa_b}})^{\mathrm{lb}} = (t_b^{(\ell)})^{-\frac{4}{\kappa_b}} - \frac{4}{\kappa_b}(t_b - t_b^{(\ell)})(t_b^{(\ell)})^{-\frac{4}{\kappa_b}-1},\quad (e_k^{-\frac{2}{\kappa_k}})^{\mathrm{lb}} = (e_k^{(\ell)})^{-\frac{2}{\kappa_k}} - \frac{2}{\kappa_k}(e_k - e_k^{(\ell)})(e_k^{(\ell)})^{-\frac{2}{\kappa_k}-1}, \tag{23b}$$

$$(x^2)^{\mathrm{lb}} = -(x^{(\ell)})^2 + 2x^{(\ell)}x,\quad (y^2)^{\mathrm{lb}} = -(y^{(\ell)})^2 + 2y^{(\ell)}y,\quad (z^2)^{\mathrm{lb}} = -(z^{(\ell)})^2 + 2z^{(\ell)}z. \tag{23c}$$

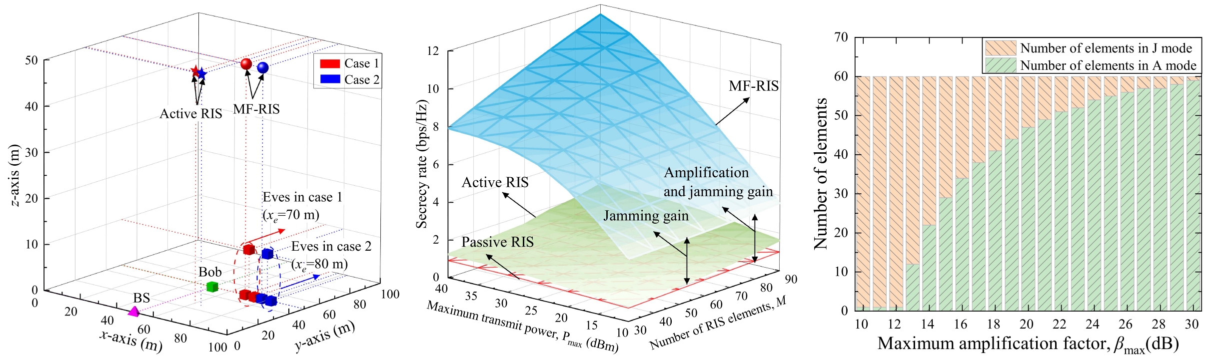

(a) (b) (c)

Fig. 2. (a) RIS deployment versus x_e. (b) Secrecy rate versus $P_{\max}$ and M. (c) Element allocation versus $\beta_{\max}$.

TABLE II
SIMULATION PARAMETERS

Parameters	Value
Location	$\mathbf{w}_0=[50,0,0]$ m, $\mathbf{w}_b=[50,50,0]$ m, $\mathbf{w}_k=[x_k,50,0]$ m, $\forall k\in\mathcal{K}/\{K\}$, $\mathbf{w}_K=[x_K,50,10]$ m
Communication	$N=2$, $K=3$, $h_0=-30$ dB, $\rho=3$ dB, $\kappa_0=\kappa_i=2.6$, $\bar{\kappa}_i=3$, $\forall i\in\{b,1,\ldots,K-1\}$, $\kappa_K=2.4$, $\bar{\kappa}_K=2.8$, $\sigma_0^2=\sigma_1^2=-90$ dBm, $P_{\text{out}}=10$ dBm

IV. SIMULATION RESULTS

In this section, numerical results are provided to demonstrate the performance of the proposed UAV-mounted MF-RIS-aided secure communication system. We consider a UAV deployable range of $\{[x,y,z]^{\text{T}}|0\leq x\leq 100, 0\leq y\leq 100, 50\leq z\leq 100\}$ m. The horizontal coordinates of Eves are randomly distributed on the line from $[x_e-3,50,0]$ m to $[x_e+3,50,0]$ m. Unless otherwise stated, we set $x_e=80$, $P_{\max}=30$ dBm, $M=60$, $P_{\text{J}}=0$ dBm, and $\beta_{\max}=10$ dB [4]. Other parameters are summarized in Table II, where $\bar{\kappa}_i$, $\forall i\in\{b\}\cup\mathcal{K}$, denote the path loss exponents of the links from the BS to Bob/Eves. For comparison, we consider the UAV-mounted passive [3] and active RISs [4] as benchmarks.

Fig. 2(a) shows the RIS deployment versus x_e. We consider case 1 with $x_e=70$ and case 2 with $x_e=80$. We reveal the deployment characteristics of different RISs by comparing their deployment changes in these two cases. It is observed that in both cases, the active RIS prefers to be deployed closer to Bob and is less affected by Eves' movement. However, the MF-RIS is deployed near Eves and often located directly above Eves. The reasons are given as follows: 1) Equipped with the capacity of emitting jamming, the MF-RIS is able to directly suppress strong illegal eavesdropping and safeguard wireless communications. 2) However, the active RIS can only mitigate eavesdropping to a limited extent while enhancing legitimate reception. This reveals the potential of the proposed MF-RIS for combating eavesdropping in the presence of multiple Eves.

Fig. 2(b) depicts the secrecy rate versus $P_{\max}$ and M. Overall, it is observed from all results that the proposed MF-RIS always outperforms the benchmarks, while the passive RIS appears to be the worst. Even in the case of low transmit power and small RIS size (e.g., $P_{\max}=10$ dBm and $M=30$), the MF-RIS can attain 2.94 and 3.69 times performance gains over active and passive RISs, respectively. For passive and active RISs, when M is fixed and $P_{\max}$ goes to ∞, the secrecy rate converges to a constant. This shows that only increasing the signal power is inefficient for security enhancement, and introducing the jamming emission function at the MF-RIS is critical.

Fig. 2(c) illustrates the RIS element allocation versus $\beta_{\max}$. When $\beta_{\max}$ is small, in order to effectively combat serious eavesdropping, the MF-RIS tends to allocate most of the elements to operate in J mode. As $\beta_{\max}$ increases, the MF-RIS expands the element size in A mode to enhance legitimate reception, due to the increase in the power of the reflected signal and the generated jamming signal. This also reveals that the proposed MF-RIS provides additional DoFs for system design, allowing us to flexibly allocate element resources according to various application scenarios.

V. CONCLUSION

This letter proposed a UAV-mounted MF-RIS architecture enabling simultaneous signal reflection, amplification, and friendly jamming. A secrecy rate maximization problem was formulated in a UAV-mounted MF-RIS assisted secure communication system by jointly optimizing the transmit beamforming and the MF-RIS deployment. Simulation results revealed that the proposed MF-RIS obtains 2.94 and 3.69 times gains over active and passive RISs, respectively.

REFERENCES

[1] W. U. Khan et al., "Opportunities for physical layer security in UAV communication enhanced with intelligent reflective surfaces," *IEEE Wireless Commun.*, vol. 29, no. 6, pp. 22–28, Dec. 2022.

[2] Y. Cao et al., "Toward smart and secure V2X communication in 5G and beyond: A UAV-enabled aerial intelligent reflecting surface solution," *IEEE Veh. Technol. Mag.*, vol. 17, no. 1, pp. 66–73, Mar. 2022.

[3] W. Wang et al., "Secrecy performance analysis of IRS-aided UAV relay system," *IEEE Wireless Commun. Lett.*, vol. 10, no. 12, pp. 2693–2697, Dec. 2021.

[4] L. Dong et al., "Active reconfigurable intelligent surface aided secure transmission," *IEEE Trans. Veh. Technol.*, vol. 71, no. 2, pp. 2181–2186, Feb. 2022.

[5] X. Guan et al., "Intelligent reflecting surface assisted secrecy communication: Is artificial noise helpful or not?" *IEEE Wireless Commun. Lett.*, vol. 9, no. 6, pp. 778–782, Jun. 2020.

[6] S. Hu et al., "Secure communication in multi-functional active intelligent reflection surface-assisted systems." May 2022. [Online]. Available: https://arxiv.org/abs/2205.02512

[7] D. Diao et al., "Enhancing reliability and security of UAV-enabled NOMA communications with power allocation and aerial jamming," *IEEE Trans. Veh. Technol.*, vol. 71, no. 8, pp. 8662–8674, Aug. 2022.

[8] X. Tang et al., "Robust secrecy via aerial reflection and jamming: Joint optimization of deployment and transmission," *IEEE Internet Things J.*, Mar. 3, 2023, early access, doi: 10.1109/JIOT.2023.3251993.

[9] Z. Wang et al., "Channel estimation for intelligent reflecting surface assisted multiuser communications: Framework, algorithms, and analysis," *IEEE Trans. Wireless Commun.*, vol. 19, no. 10, pp. 6607–6620, Oct. 2020.

[10] P. Cao et al., "A sequential constraint relaxation algorithm for rank-one constrained problems," in *Proc. 25th Eur. Signal Process. Conf. (EUSIPCO)*, Kos, Greece, Aug. 2017, pp. 1060–1064.

[11] X. Mu et al., "Exploiting intelligent reflecting surfaces in NOMA networks: Joint beamforming optimization," *IEEE Trans. Wireless Commun.*, vol. 19, no. 10, pp. 6884–6898, Oct. 2020.